



Evaluation of New High Entropy Alloy as Thermal Sprayed Bondcoat in Thermal Barrier Coatings

Xinqing Ma¹ · Peter Ruggiero¹ · Rabi Bhattacharya² · Oleg N. Senkov² · A. K. Rai²

Submitted: 8 July 2021 / in revised form: 21 September 2021 / Accepted: 3 November 2021 / Published online: 1 December 2021
© ASM International 2021

Abstract High-entropy alloys (HEAs) have great potential to be used as high-temperature materials and in coating material applications due to their combination of strength, ductility, thermal stability, wear, and oxidation resistance. In this work, a new HEA alloy based on NiCoCrAlSi composition was designed and deposited into metallic coatings by high-velocity oxy-fuel (HVOF) and air plasma spray (APS) processes, with the aim of developing new HEA bondcoats for thermal barrier coating (TBC) systems. The HEA coatings were analyzed for phases, microstructure and composition using X-ray diffraction (XRD), scanning electron microscopy (SEM), and energy dispersive spectroscopy (EDS). The results showed that the BCC phase is the major phase present in the as-applied HVOF coating that was vacuum diffusion treated at 1080 °C. APS coatings of the same composition HEA alloy showed a two-phase structure consisting of the L12 and BCC/B2 phases. The HEA bondcoats produced by HVOF were tested for oxidation resistance at 1050 °C in air, and for

thermal cycling resistance of the TBC comprising of the HVOF-applied HEA bondcoat and standard 8YSZ ceramic topcoat. The results showed internal oxidation in the HEA bondcoat during the high-temperature oxidation exposure, but no significant coating failure after 100 thermal cycles at 1150 °C.

Keywords bondcoat · coating characterization · high-entropy alloys phase structure · thermal barrier coating · thermal spray

Introduction

Thermal barrier coatings (TBCs) for high-temperature operation of propulsion and power generation systems have enabled substantial improvements in the performance and efficiency of gas turbine engines. A typical TBC comprises a metallic bondcoat for high-temperature oxidation protection of the substrate and a ceramic topcoat layer for thermal barrier insulation purposes [1–5]. The bondcoat serves two primary functions: (1) to improve the adherence of the TBC and (2) to protect the substrate from environmental attack if the topcoat does spall. This is achieved by making the bondcoat composition such that it is a reservoir from which elements such as Al can diffuse outward to form a protective α -Al₂O₃ thermally grown oxide (TGO) layer while maintaining cohesion with the topcoat without reacting with it. The TGO layer should remain elastic to the highest operating temperatures and not creep to prevent “rumpling” or cavitation during thermal cycling that can lead to the development of local separations at the TGO/TBC interface. At the same time, a TBC has to operate at the highest temperature possible to minimize the amount of air used to cool the critical hot-section components such as

This article is part of a special topical focus in the Journal of Thermal Spray Technology on High Entropy Alloy and Bulk Metallic Glass Coatings. The issue was organized by Dr. Andrew S.M. Ang, Swinburne University of Technology; Prof. B.S. Murty, Indian Institute of Technology Hyderabad; Distinguished Prof. Jien-Wei Yeh, National Tsing Hua University; Prof. Paul Munroe, University of New South Wales; Distinguished Prof. Christopher C. Berndt, Swinburne University of Technology. The issue organizers were mentored by Emeritus Prof. S. Ranganathan, Indian Institute of Sciences.

✉ Xinqing Ma
xinqing.ma@cwst.com

¹ Surface Technologies Division, Curtiss-Wright Corporation, East Windsor, CT, USA

² UES Inc., Dayton, OH, USA

vanes and blades, without reacting with the underlying substrate material, which is Ni-base superalloy typically for high-temperature turbine engines. Overlay coatings of MCrAlY, where M is either Ni, Co, or a mixture of these elements are generally used as bondcoats. The metallic bondcoats are generally applied by thermal spray, mostly plasma spray, and high-velocity oxy fuel spray.

The drive toward higher efficiency engines is demanding higher performance TBC coatings, both bondcoat and topcoat. High-entropy alloys (HEAs) have the potential to be used as high-temperature materials and in coating material applications due to their combination of strength, ductility, thermal stability, wear, and oxidation resistance [6–8]. HEAs typically refer to alloys that are comprised of five or more elements, at or near equi-atomic composition. Some of these alloys are solid solution alloys on simple underlying lattices such as face-centered cubic (FCC) or body-centered cubic (BCC). The basic principle behind HEAs is that solid-solution phases are stabilized by their significantly high entropy of mixing compared to intermetallic compounds, especially at high temperatures. This allows them to be synthesized and manipulated to result in possible compositions and combinations of properties required for a metallic bondcoat. Several HEAs have been shown to have very sluggish diffusion kinetics [9, 10] and improved oxidation resistance in their bulk form [11]. Not much work has been done on coating deposition of HEAs, in particular, for applications as bondcoats in TBC systems. Meghwal et al. reviewed the early-stage development works for thermal spray HEA feedstock materials and coatings, as well as coating properties of friction, corrosion and oxidation [12]. Thermal spray processes including plasma spray, HVOF and cold spray (CS) had been employed to manufacture those HEA alloy coating. Hsu et al. developed an overlay coating of NiCoFeCrSiAlTi HEA alloy by APS process [13, 14]. The as-deposited HEA coating has a phase structure of supersaturated BCC with some oxide stringers formed during the APS process. The oxidation test demonstrates that the coating exhibits oxidation resistance as good as typical NiCrAlY coating. Huang et al. have studied the HEA coatings of the compositions of AlSiTiCrFeCoNiMo_{0.5} and AlSiTiCrFeNiMo_{0.5} alloys deposited by thermal spray [15]. The as-sprayed coatings showed the same primary phase as the as-cast alloys except that the X-ray intensities of coatings were much lower than those from as-cast alloys. This was interpreted as due to rapid solidification induced saturation in solute concentration resulting in severe lattice distortion in the simple solution phase of BCC structure. It was found that the hardness of the as-sprayed material was about one-half of the hardness in the as-cast state. The authors stated that this is reasonable since hard phases were

inhibited by rapid solidification and lost their contributions in precipitation strengthening and composite strengthening.

Aging at high temperatures up to 1100 °C resulted in an increase in hardness closer to the as-cast values. Oxidation studies revealed good oxidation resistance up to 1000 °C. The oxidation protection was due to the formation of aluminum and or chromium oxides. Recently, Yue et al. have fabricated an AlCoCrCuFeNi HEA coating using a two-step method involving plasma spray processing and laser re-melting for application on Mg alloys for corrosion resistance [16]. The as-sprayed coating was found to contain micro-porosity that disappeared after laser re-melting. The XRD results showed that both the as-sprayed and the laser re-melted coatings were composed of a BCC solid solution phase with a small amount of FCC phase, and no intermetallic compounds were found. The laser melting method was reviewed by Zhang et al. to modify microstructures of HEA alloy layers to achieve different properties [17]. The coating demonstrated increasing hardness after holding at temperatures in the range of 400–700 °C compared to the as-produced state. This was explained by the decomposition of a supersaturated solid solution and the formation of intermetallic precipitates. Thus, it is clear that the previous studies on HEA coatings did not directly address the requirements of bondcoats for TBC systems.

In this paper, we report the development of HEA alloy bondcoats for TBC systems using novel high-temperature HEA compositions. The selection of alloy composition was made from thermodynamic calculations. High-velocity oxy-fuel (HVOF) and atmospheric plasma spray (APS) processes were used to deposit the coatings.

Experimental

High Entropy Alloy Powder

Firstly, calculations of the equilibrium phase diagram of Al_x(Co,Cr,Ni)_{88-x}Si₂ system for 8%<x<35% and 26%<x<50% was conducted to determine a composition range where no phase transformation occurs (details to be described in result section). Thermodynamic modeling using CALPHAD (CALculation of PHase Diagrams, thermodynamic databases developed by CompuTherm LLC) was used for calculating the HEA phase diagram as described in the references [18, 19]. Then, powders of Al₃₀Co₂₂Cr₂₃Ni₂₃Si₂ (at.%) of two sizes, – 75/+45 μm and – 45/+20 μm were obtained from F. J. Brodmann & Co., L.L.C., made by a method of mechanical alloying according to the supplier. Post thermal treatment for the powders at 1250 °C for 6 h was conducted mainly for particle sintering, diffusion, densification, and chemical

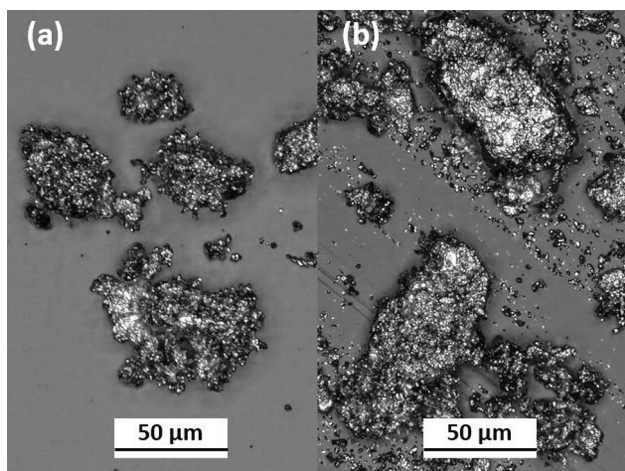


Fig. 1 Morphologies of the HEA powders made by the mechanical alloying method. (a) Powder size $-45/+20\ \mu\text{m}$ and (b) powder size $-75/+45\ \mu\text{m}$

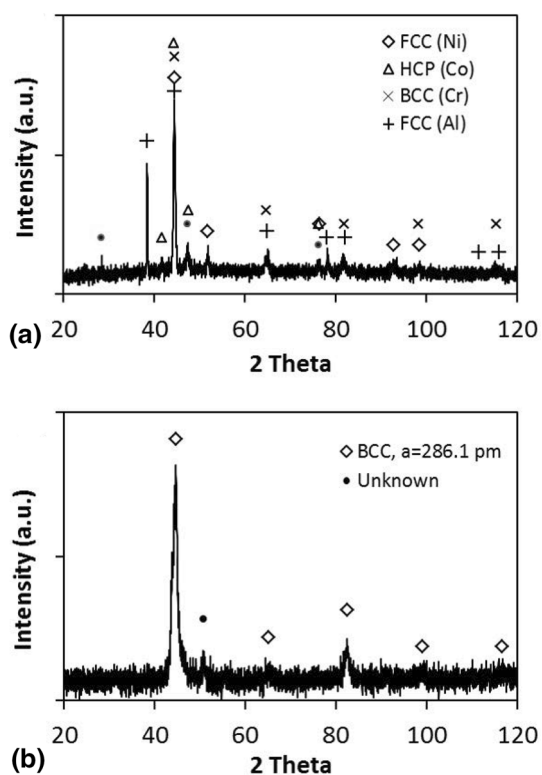


Fig. 2 X-ray diffraction patterns taken from (a) mechanically alloyed elemental powder and (b) a sample of the $\text{Al}_{30}\text{Co}_{22}\text{Cr}_{23}\text{Ni}_{23}\text{Si}_2$ (at.%) HEA sintered from the powder

homogeneity. The morphologies of the two powders are shown in Fig. 1. They are non-spherical powders and are characterized by a fine-grained agglomeration structure. X-ray diffraction (XRD) analysis revealed that the powder samples consisted of a mixture of the pure elements (Fig. 2a). However, after sintering these powders at $1250\ ^\circ\text{C}$ for 6 hrs in a high-purity argon, the diffraction peaks

from pure elements disappeared and an essentially single-phase BCC structure, with the lattice parameter $a = 286.1\ \text{pm}$ synthesized (Fig. 2b). A diffraction peak at $2\Theta = 50.7^\circ$ ($d = 179.9\ \text{pm}$), which does not belong to the BCC phase indicates the presence of a minor secondary (likely silicide) phase in the produced HEA powder.

Thermal spray

HEA coating specimens were produced by Curtiss-Wright Surface Technologies (“CWST”) using a Jet Kote-3000 HVOF torch (Stellite, Goshen, IN) and a 7MB plasma torch (Metco, Westbury, NY) for the HEA bondcoats. For TBC test specimens, 8YSZ topcoat was sprayed onto the HVOF-formed HEA bondcoat using the same 7MB plasma torch. Coatings were deposited by APS spray of $\text{Al}_{30}\text{Co}_{22}\text{Cr}_{23}\text{Ni}_{23}\text{Si}_2$ (at.%) with powder size of $-75/+45\ \mu\text{m}$. HVOF Spray of $\text{Al}_{30}\text{Co}_{22}\text{Cr}_{23}\text{Ni}_{23}\text{Si}_2$ (at.%) was used for powder size of $-45/+20\ \mu\text{m}$. Primary optimized parameters used for the APS HEA coating include Ar at 55Psi/100 SCFH, H_2 at 55Psi/20 SCFH, Current 500A and volt 75V, standoff distance 100 mm; and for the HVOF HEA coating include H_2 at 120 Psi/68 FMR, O_2 at 120Psi/34 FMR, standoff distance 150 mm. Coatings were post heat-treated at $1080\ ^\circ\text{C}$ for 4 hrs in vacuum for diffusion bonding and compositional homogeneity by following an internal annealing treatment procedure for a typical MCrAlY coating. All coatings were deposited on one side of 1-inch (25.4 mm) diameter discs of Haynes[®] 230 alloy. The typical coating thickness is about 200–250 μm . Coatings were analyzed for phase, microstructure and composition using x-ray diffraction (XRD) and scanning electron microscopy with energy dispersive x-ray analysis (SEM/EDS).

Oxidation and Thermal Cycling Test

Internal test procedures for TBC evaluation were developed and used for isothermal oxidation and thermal cycling of the HVOF-formed HEA bondcoats and TBCs in a CWST facility. The HEA bondcoats and TBC samples made by HVOF were used in both tests. The isothermal test was tested at $1050\ ^\circ\text{C}$ for 200 hrs in air, and for thermal cycling test of the HEA bondcoat with standard 8YSZ topcoat up to 100 cycles which are composed of 1 hr at $1150\ ^\circ\text{C}$ and cooling with an air jet to room temperature within 15 minutes by following an internal test procedure for TBC-type coatings. The tested TBC samples were examined on the coating surfaces after completion of each cycling at room temperature, respectively. As a rule of thumb, the spallation percentage of more than 30% is considered as coating failure.

Results and Discussion

HEA Alloy Compositional Design

The technical approach was to synthesize HEA alloys with compositions that have the following characteristics:

- High oxidation resistance: Must produce thermally grown oxide (TGO), α -Al₂O₃ stabilized with α -Cr₂O₃. Thus, the alloy must contain sufficient amounts of Al and Cr.
- Strong bond with the substrate: Since the substrates are Ni-based alloys, the HEA alloy should contain Ni or elements forming extended solid solutions with Ni (Co, Cr, Cu, Fe, Mn, Pd, Pt).
- High fracture toughness: The alloy must contain a sufficient amount of ductile solid solution phase.
- High hardness and wear resistance: The alloy must contain a sufficient volume fraction of hard intermetallic phases, preferably as fine, homogeneously distributed precipitates. The goal is to produce an alloy with a fine mixture of two coherent phases, one of which is a disordered BCC crystal structure and another is an ordered B2 crystal structure. The mixture of these two phases will provide the necessary combination of mechanical properties (hardness, wear resistance and toughness). Age hardenable composition is one of the possibilities.
- Similar coefficient of thermal expansion (CTE) with substrate and topcoat.
- High thermal stability: No first-order phase transformations in the temperature range of use.

In order to find a composition range where no phase transformation occurs, we conducted calculations of the equilibrium phase diagram of Al_x(Co,Cr,Ni)_{88-x}Si₂ system for 8% < x < 35% and 26% < x < 50%, as shown in Fig. 3. The results show that there is a wide composition-temperature range, where no phase transformations occur in the Al_x(Co,Cr,Ni)_{88-x}Si₂ system. Here, Al can vary from 31 to 42 at.% and temperature from 500 to 1300 °C retaining the same phase content: B2+BCC+M₃Si. We believe that the alloys in this composition range should be a good choice for coatings, because oxidation, as well as heating and cooling cycles, would not cause any phase transformations. Thus, we have identified Al₃₀Co₂₂Cr₂₃Ni₂₃Si₂ (at.%) alloy from the analysis as a promising alloy for the HEA bondcoat.

Microstructure of HEA Coatings

Figure 4 shows the optical views of the cross-sections of the HEA coatings deposited by APS and HVOF separately

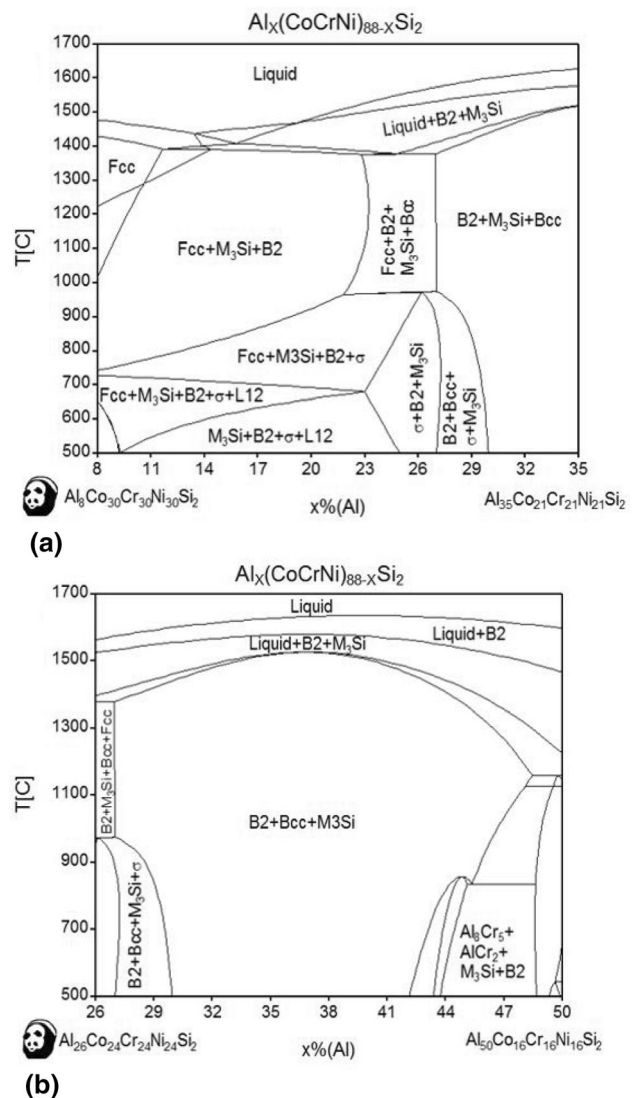


Fig. 3 Equilibrium phase diagram of (a) Al_x(Co,Cr,Ni)_{88-x}Si₂ alloy for 8% < x < 35% and (b) Al_x(Co,Cr,Ni)_{88-x}Si₂ alloy for 26% < x < 50%

with a typical coating thickness of 200–250 μm. In Fig. 4(a), the APS-sprayed bondcoat consists of lamellar splats with the presence of some micro-porosity and oxides, which are typical features resulting from plasma spray methods. The APS-sprayed coating seems to be uniform without large unmelts. In Fig. 4(b), the HVOF-sprayed bondcoat consists of not quite visible lamellar splats, but with the presence of many small pores and some large unmelts. It is believed that the small-sized porosity comes from the originally milled feedstock powders which are not fully packed with milled fine particles containing a lot of small porosity, as well as a low degree of melting of the powder feedstock in the HVOF process. The existence of large unmelts in the coating also should be attributed to the

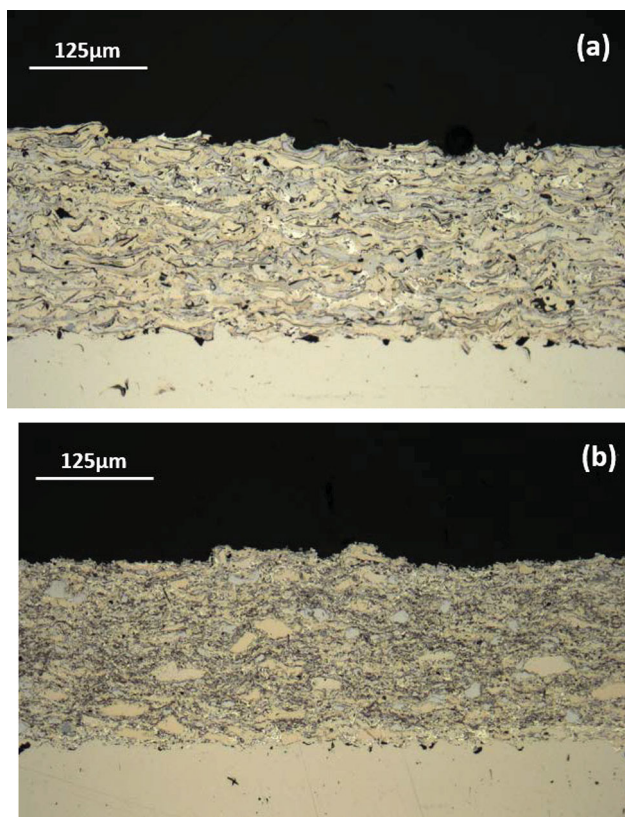


Fig. 4 Optical views of the cross-section of the HEA coatings: (a) APS spray, powder size – 75/+45 μm and (b) HVOF spray, powder size – 45/+20 μm

partial melting of some powder particles, which is often observed in HVOF-spray coating.

Since the APS-formed HEA coatings showing the unfavorable phase-constitution (major FCC+ minor BCC +B2 + in-flight oxidation) were not investigated any further, but with a focus on the HVOF-formed HEA coating. Secondary electron (SE) and backscatter electron (BSE) images of the HEA coating deposited on the Haynes 230 substrate using HVOF method are shown in Fig. 5. Note two characteristic layers of the coating. The bottom layer, which is in contact with the substrate, is denser than the top layer. Microstructure is representative of standard MCrAlY bond coat deposited by HVOF process likely due to “peening” effect. It is believed that a more uniform coating could be obtained with further optimized process condition. Coating-substrate interface appears adhesive to the substrate and free from pores and separation.

Phase Analysis of HEA Coating

Figure 6 shows XRD patterns of the APS and HVOF-formed coatings, respectively, after vacuum diffusion treatment at 1080 $^{\circ}\text{C}$ for 4 hrs. The APS coating has a two-phase structure consisting of the FCC and BCC (or B2)

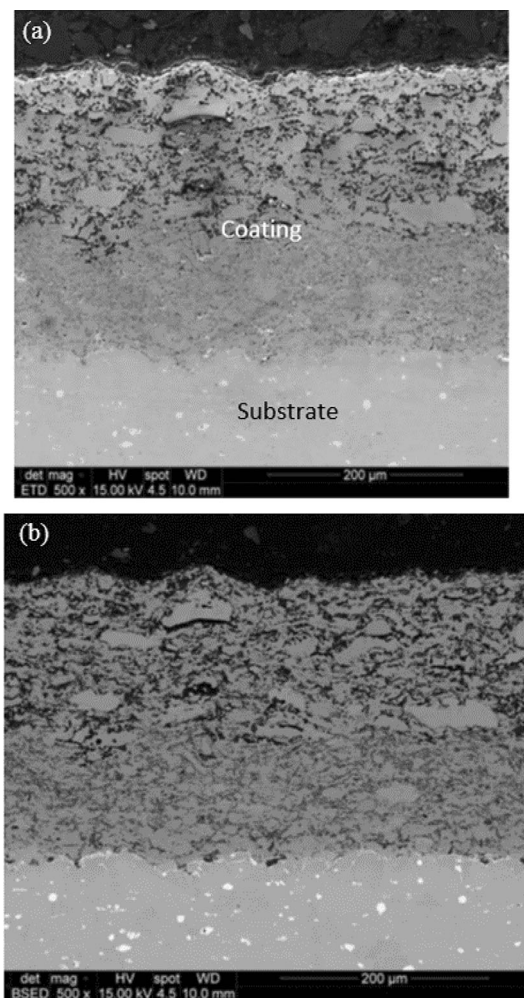


Fig. 5 Cross-section SEM images of HVOF $\text{Al}_{30}\text{Co}_{22}\text{Cr}_{23}\text{Ni}_{23}\text{Si}_2$ HEA coating: (a) secondary electron image and (b) backscatter electron image

phases. Based on peak intensity analyses of the FCC and BCC phases, the volume fraction of FCC phase seems to be comparable with that of BCC. A small amount of Cr-doped alumina is also recognized. Similarly, Xue et al reported that the FeCoNiCrAl and FeCoNiCrMn coatings by APS was composed of micro-nano face-centered cubic (FCC) and body-centered cubic solid solutions (BCC) and a small amount of band-like micro-nano alumina formed during plasma spraying, and the FeCoNiCrMn coating was composed of only face-centered cubic solid solution (FCC) and dispersed nanocrystalline oxide ($\text{Mn}_{1.5}\text{Cr}_{1.5}\text{O}_4$) [20]. It seems that the phase compositions of a HEA coating are quite dependent on HEA compositions.

The major phase in the HVOF coating is BCC/B2. Small peaks from FCC phase and Al_2O_3 are also identified (Fig. 6b). The ordered B2 phase is recognized by the presence of a super-lattice (001) peak at $2\theta = 31.18^{\circ}$. High intensity of the fundamental diffraction peaks from BCC/

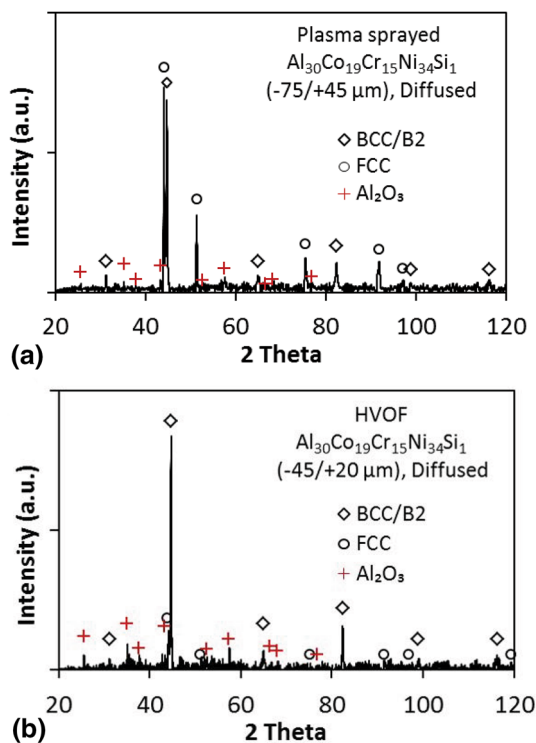


Fig. 6 X-ray diffraction patterns are taken from $\text{Al}_{30}\text{Co}_{22}\text{Cr}_{23}\text{Ni}_{23}\text{Si}_2$ (at.%) coatings after vacuum diffusion treatment at 1080 °C for 4 h: (a) APS spray and (b) HVOF spray

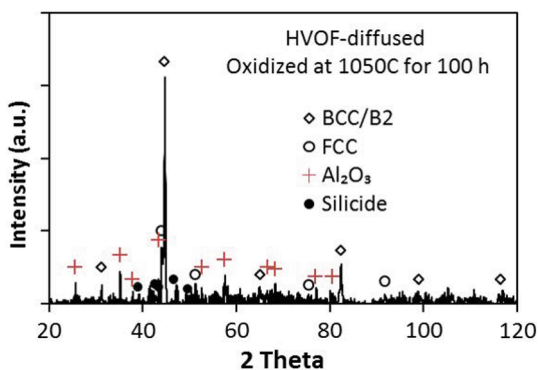


Fig. 7 XRD spectrum of HVOF-deposited $\text{Al}_{30}\text{Co}_{22}\text{Cr}_{23}\text{Ni}_{23}\text{Si}_2$ coating after isothermal oxidation at 1050 °C for 100 h in air

B2 indicates that this phase is the major phase in the HVOF sample. Compared to the XRD spectra of the powder particles that showed the characteristics of an elemental mixture, the sprayed and bonded coating shows that it is an alloy with a primary BCC/B2 phase characteristic of the HEA composition.

Isothermal Oxidation Test

Oxidation tests of the HVOF-formed HEA coatings were performed in a box furnace at 1050 °C for 50, 100 and 200 hrs in atmospheric air. XRD patterns of the HEA coatings

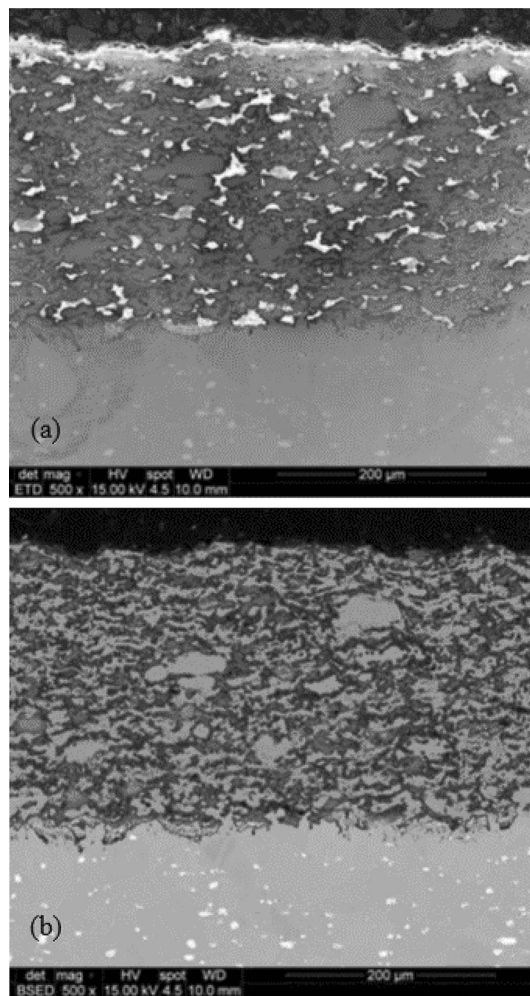


Fig. 8 HVOF coating is made of a high entropy alloy (HEA) after oxidation at 1050 °C for 50 hrs. (a) Secondary electron and (b) backscatter electron SEM images

after oxidation showed minimal change from the as-deposited pattern. Figure 7 shows the XRD pattern of a sample oxidation tested at 1050 °C for 100 hrs. Compared to the XRD spectrum of as-deposited coating in Fig. 6(b), very little change can be observed after oxidation. Primary BCC/B2 phase along with small peaks of FCC and Al_2O_3 is presented after oxidation. These results indicate that the coating is thermally stable and Al_2O_3 -type TGO is primarily grown on the surface of the HEA coating during the oxidation test. Excellent oxidation resistance of the thermal sprayed HEA coatings has displayed potential in replacing conventional bond coat materials [21, 22]. Ma et al studied the oxidation behavior of the $\text{CoCr}_2\text{FeNb}_{0.5}\text{Ni}$ high-entropy alloy coatings with and without Si via laser cladding in $\text{N}_2\text{-}44\text{CO}_2\text{-}6\text{H}_2\text{O}$ gas at 800 °C. It was found that Si atoms can be doped into Laves phase and improve the phase stability by reducing the spacing of the crystal plane. The addition of Si improves the high-temperature oxidation

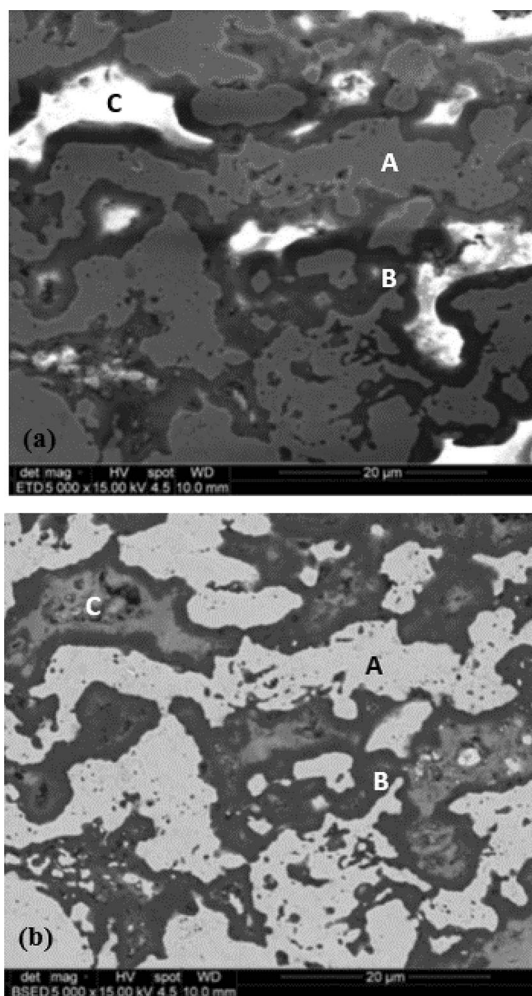


Fig. 9 HVOF coating is made of a high entropy alloy (HEA) after oxidation at 1050 °C for 50 hrs. (a) Secondary electron and (b) backscatter electron SEM images of the coating showing three distinguished constituents: Non-oxidized particles (A), Al₂O₃ oxide (dark phase adjacent to the particles) (B), and pores (C) (shown as bright regions on the SE image)

resistance since the (Cr, Si)O_x amorphous oxide layer can prevent oxygen from diffusing inward [23]. Therefore, it is believed that the stable phase structure in our tested HEA samples can also be explained by the addition of Si in the NiCoCrAlSi HEA system.

To further investigate the oxidation behavior of the HVOF HEA coating, the oxidized specimens were closely examined using SEM/EDAX analyses. Figs. 8(a) and (b) show SE and BSE images of the HVOF HEA coating after oxidation at 1050 °C for 50 hrs in air. The coating consists of (1) non-oxidized particles of original material (they are gray color) in Fig. 8(a), (2) oxide layer on the surfaces of the deposited particles (oxide is of dark color) in Fig. 8 and (3) mixed oxide phase (very bright color) in Fig. 8(a). Higher magnification SE and BSE images of the same are shown in Fig. 9. Three clearly distinguished

Table 1 Representative chemical compositions (in at.%) of regions indicated in Fig. 9 by letters A, B and C

Element	O	Al	Co	Cr	Ni	Si
Particles (A)	2.01	1.07	42.43	17.21	35.25	2.03
Oxide (B)	50.34	44.96	1.25	2.34	0.88	0.23
Mixed Oxide (C)	36.52	24.77	13.78	9.09	5.14	10.7

constituents are identified as: non-oxidized particles (A), Al₂O₃ oxide (dark phase adjacent to the particles) (B), and mixed oxide phase (C) (shown as bright regions on the SE image). Table 1 shows the representative composition of the phases identified on selected phase areas in Fig. 9. In the particles area A, high metallic elements (Co, Cr, Ni) and low O and Al contents are identified, showing thin TGO formed. In the oxide area B, high O and Al contents but low Co, Cr and Ni contents are determined, indicating high purity Al₂O₃ TGO is grown. In the area C, all alloy elements are detected and indicate the formation of mixed oxides, possibly include the (Cr, Si)O_x oxide as reported in reference [23]. Hsu et al investigated the overlay coating of NiCo_{0.6}Fe_{0.2}Cr_{1.5}SiAlTi_{0.2} (C3) via APS and its oxidation at 800 and 1100 °C [14]. The oxidation weight gain result demonstrated that the coating exhibited oxidation resistance as good as typical NiCrAlY coating at 1100 °C due to the formation of a dense thermally grown oxide layer (TGO) comprising Al₂O₃ and Cr₂O₃.

Fig. 10 shows the SEM images of the 1050 °C for 200 hrs oxidized sample. Thickness of the coating remained unchanged and no measurable thin oxide layer on the top of the surface, but visible internal oxidation was found. It is assumed that the initial TGO layer was formed but not sufficient to stop the competitive formation of internal oxide in the coating. After internal oxidation occurred, the TGO growth on surface was suppressed due to a lack of outward diffusion supply of TGO elements such as Al and Cr. A darker layer between substrate and coating is likely an artifact caused by poor sample preparation (cleaning and drying after polishing). The gray particles in Fig. 10(b) are original non-oxidized particles. The dark regions between the particles are aluminum oxide doped with other alloying elements. The microstructures were analyzed in details at higher magnifications and will be described in future publications.

Thermal cycling Test

The TBC specimens with the HVOF-deposited HEA bondcoat were exposed to laboratory thermal cycle testing was conducted manually in a box furnace at 1150 °C (± 10 °C) in air. A 60 min isothermal hold at 1150 °C and forced

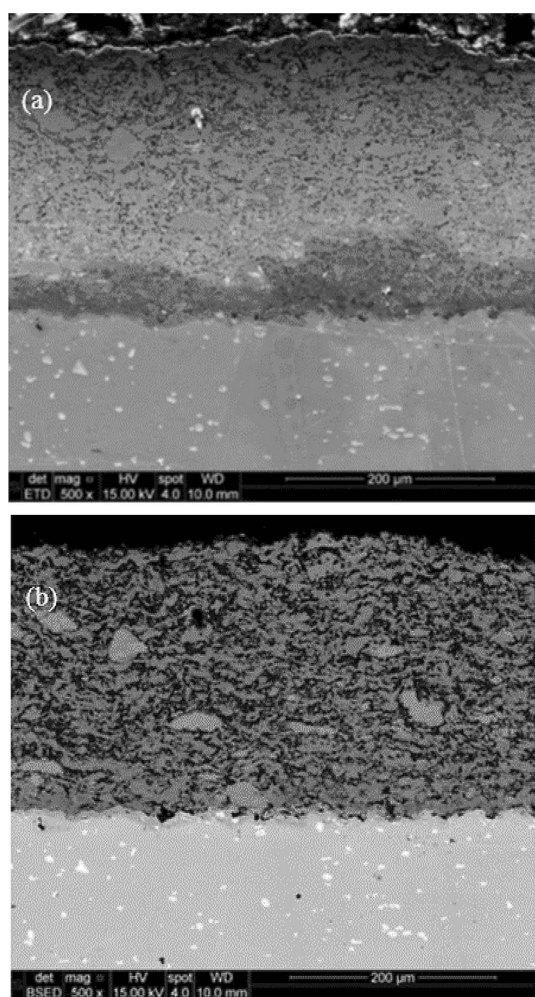


Fig. 10 (a) Secondary and (b) backscatter electron images of coating and substrate after oxidizing at 1050 °C for 200 hrs

air cooling to room temperature for 15 min after the sample was transferred to a cold stage was used as the cycle parameters. Specimens were visually inspected after each cycle and weight was measured after every 10 cycles. Fig. 11(a) shows the microstructures of the TBC samples before and after the cyclic oxidation test at 1150 °C in air after 100 cycles, as well as top views of the test samples in Fig. 11(b). No spallation or damage of the TBC was observed from the top view of the tested TBC sample, but the microstructure of the tested TBC indicates that the topcoat tends to crack and separate locally within the ceramic topcoat near the interface of the topcoat and HEA bondcoat. Weight gain chart in Fig. 11(b) shows no additional weight gain after the initial (transient oxidation stage) gain of about 0.2 mg/cm². This result can be directly compared with that of Haynes et al [24] where various MCrAlY bond coats with standard YSZ top coat on one side of Rene N5 substrate was evaluated in an exactly similar manner. Their reported weight gain after 100 cycles

was higher than 1mg/cm². In conclusion, based on the results of oxidation weight gain and thermal cycling resistance, the new HEA bond coat has the potential to significantly increase the life of the standard APS YSZ top coat compared with the current MCrAlY bond coat/YSZ TBC at about equal cost after further coating optimization is performed.

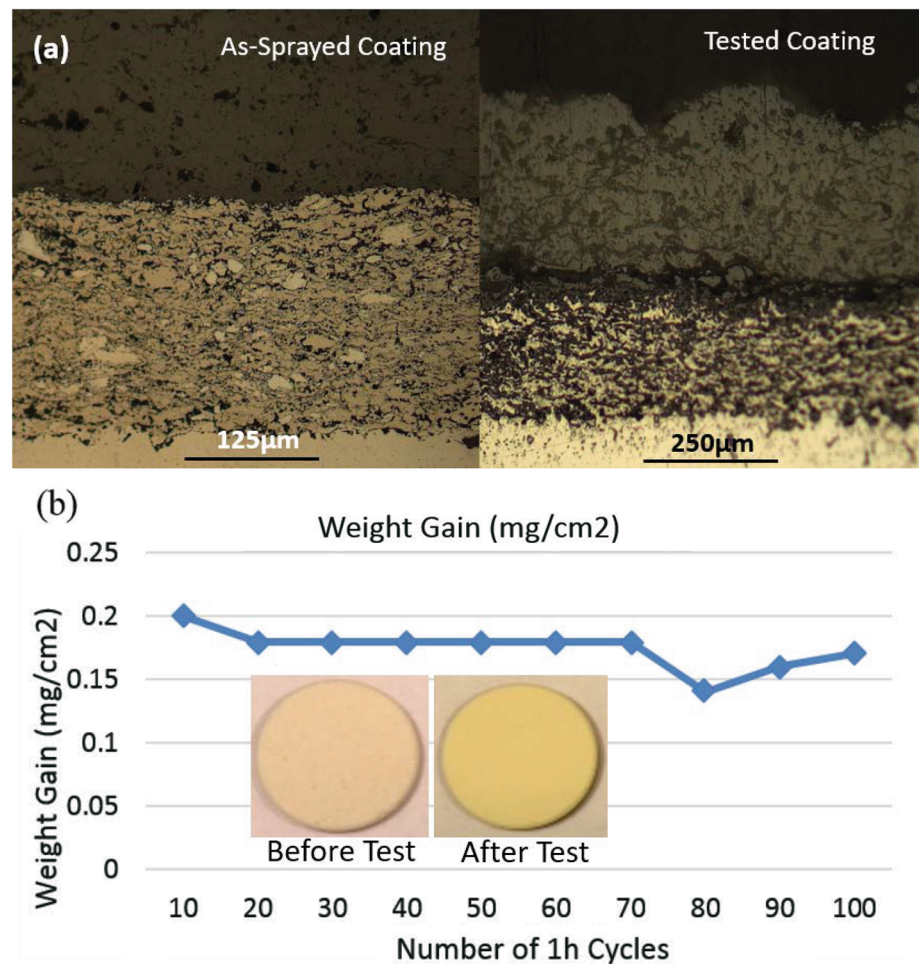
In the present work, the initial investigation on phase structures indicated the Al₃₀Co₂₂Cr₂₃Ni₂₃Si₂ HEA alloy a good candidate for metallic overlay or bondcoat and the effect of HEA alloy design, and thermal spray process. The addition of Si in the HEA alloy is beneficial for oxidation resistance as revealed in the similar study [23]. The APS and HVOF-formed coatings have different phase compositions, and the HVOF coating has a thermally stable BCC phase structure. It also is believed that the quality and types of powder feedstock have a direct impact on the resultant coatings and their oxidation behaviors of the HEA coatings. The mechanical alloying conditions such as milling speed, duration, media, and quantity as well as thermal treatment parameters can be further optimized for better chemical homogeneity and phase control. Additionally, the improvement on the feedstock density and particle shape will result in good powder flowability and desirable coating microstructure. Internal oxidation was found during both the oxidation tests, which is unfavorable for oxidation resistance and coating longevity, therefore, the coating quality should be further improved by optimizing feedstock materials, process parameters, and post-treatment such as annealing and laser remelting as reviewed in literatures [25–28].

Conclusions

The present work aimed to test and characterize a novel high entropy alloy bondcoat for thermal barrier coatings. The main results are summarized as:

- New high entropy alloy (HEA) composition of Al₃₀Co₂₂Cr₂₃Ni₂₃Si₂ (at.%) was selected from thermodynamic calculations based on the requirements of a thermally stable solid solution alloy with a predominantly BCC structure.
- Bulk alloy of selected material was synthesized and fully characterized to demonstrate HEA formation.
- HEA bondcoats have been developed to provide durability to thermal barrier coating system (TBC) for gas turbine engine components. Results of this research clearly show promise of a superior oxidation-resistant HEA bond coat as compared to standard MCrAlY bond coats.

Fig. 11 Results of thermal cycle tests of HVOF HEA bond coat with YSZ topcoat: (a) microstructures of the TBC samples before and after 100 thermal cycles at 1150 °C, (b) chart of weight gain during testing, and top views of the TBCs before and after the test. Note that only one face of the TBC specimens was coated



- Air plasma spray (APS) and high-velocity oxy-fuel (HVOF) coating deposition processes were utilized to manufacture the HEA coatings. APS coatings showed a mixture of FCC and BCC phases in nearly equal amounts while the HVOF coating showed primarily BCC phases.
- HVOF Spray was done by using a powder alloy composition of $\text{Al}_{30}\text{Co}_{22}\text{Cr}_{23}\text{Ni}_{23}\text{Si}_2$ (at.%) produced by mechanical alloying. Coatings were first heat treated to 1080 °C for 4 hrs in vacuum for diffusion bonding. The HVOF coatings were predominantly BCC/B2 phase. These coatings were dense near the interface with the substrate but had porosity away from the interface. This has resulted in oxidation around the particle splats after exposure at 1050 °C in air up to 200 hrs thus densifying the coating. Besides the internal oxidation around the splat particles, no other change in microstructure or phase content was found after the oxidation test.
- Thermal cycling test of the HVOF bond coat with standard yttria-stabilized zirconia (YSZ) TBC as the top coat showed no spallation after 100 cycles at 1150

°C in air. Minimal weight gain after the first 10 cycles and then remaining at the same level clearly indicate the slow rate of growth of the thermally grown oxide (TGO) layer.

- The results of this initial study emphasize the importance of optimizing the HEA composition, powder manufacture and coating deposition process to fully define the capability and limitations of HEAs for the bondcoat in TBC application.

Acknowledgments This work was financially supported by the department of energy's (DOE) Small Business Innovative Research Program, Grant No. DE-SC0013213. We thank Dr. Patcharin Burke, DOE Program Manager, for useful discussions.

References

1. D.R. Clarke, M. Oechsner and N.P. Padture, Thermal-barrier coatings for more efficient gas-turbine engines, *MRS Bull.*, 2012, 37, p 891–898.

2. Y. Tamarin, Protective Coatings for Turbine Blades, ASM International, (2002).
3. X. Ma et al., Low thermal conductivity thermal barrier coating deposited by the solution plasma spray process, *Surf. Coat. Technol.*, 2006, **201**(7), p 4447–4452.
4. S.M. Meier and D.K. Gupta, Evolution of thermal barrier coatings in gas turbine engine applications, *J. Eng. Gas Turbines Power*, 1994, **116**(1), p 250–257.
5. X. Ma, K. Rivellini, P. Ruggiero and G. Wildridge, Evaluation and characterization of a durable composite phase thermal barrier coating in solid particle erosion and burner rig tests, *J. Therm. Spray. Technol.*, 2021, **30**, p 69–80.
6. S. Wang, Atomic structure modeling of multi-principal-element alloys by the principle of maximum entropy, *Entropy*, 2013, **15**(12), p 5536–5548.
7. E.P. George, D. Raabe and R.O. Ritchie, High-entropy alloys, *Nat. Rev. Mater.*, 2019, **4**, p 515–534.
8. Y. Zhang and R. Li, New advances in high-entropy alloys, *Entropy*, 2020, **15**(22), p 1158–1165.
9. K. Tsai, M. Tsai and J. Yeh, Sluggish diffusion in Co-Cr-Fe-Mn-Ni high-entropy alloys, *Acta Mater.*, 2013, **61**, p 4887–4897.
10. B.S. Murty, J.W. Yeh and S. Ranganathan, *High entropy alloys*, London, Butterworth-Heinemann, UK, 2014.
11. Y. Zhang, T. Zuo, Z. Tang, M. Gao, K.A. Dahmen, P.K. Liaw et al., Microstructures and properties of high-entropy alloys, *Prog. Mater. Sci.*, 2014, **61**, p 61–93.
12. A. Meghwal, A. Anupam, B.S. Murty, C.C. Berndt, R.S. Kottada and A. Ang, Thermal spray high-entropy alloy coatings: A Review, *J. Therm. Spray Tech.*, 2020, **29**, p 857–893.
13. W.L. Hsu, H. Murakami, J.W. Yeh, A.C. Yeh and K. Shimoda, On the study of thermal-sprayed Ni_{0.2}Co_{0.6}Fe_{0.2}CrSi_{0.2}AlTi_{0.2} HEA overlay coating, *Surf. Coat. Technol.*, 2017, **316**, p 71–74.
14. W.L. Hsu, Y.C. Yang, C.Y. Chen and J.W. Yeh, Thermal sprayed high-entropy NiCo_{0.6}Fe_{0.2}Cr_{1.5}SiAlTi_{0.2} coating with improved mechanical properties and oxidation Resistance, *Intermetallics*, 2017, **89**, p 105–110.
15. P.K. Huang, J.W. Yeh, T.T. Shun and S.K. Chen, Multi-principal-element alloys with improved oxidation and wear resistance for thermal spray coating, *Adv. Eng. Mater.*, 2004, **6**(1–2), p 74–78.
16. T.M. Yue, H. Xie, X. Lin, H. Yang and G. Meng, Microstructure of laser re-melted AlCoCrCuFeNi high entropy alloy coatings produced by plasma spraying, *Entropy*, 2013, **15**(7), p 2833–2835.
17. C. Zhang, J. Zhu, H. Zheng, H. Li, S. Liu and G.J. Cheng, A review on microstructures and properties of high entropy alloys manufactured by selective laser melting, *Int. J. Extrem. Manuf.*, 2020, **2**(032003), p 1–22.
18. R. Sonkusare, P.D. Janani, N.P. Gurao, S. Sarkar, S. Sen, K.G. Pradeep and K. Biswas, Phase equilibria in equiatomic CoCu-FeMnNi high entropy alloy, *Mater. Chem. Phys.*, 2018, **210**, p 269–278.
19. B. S. Murty, J. W. Yeh, S. Ranganathan and P. P. Bhattacharjee, Alloy design in the 21st century: ICME, materials genome, and artificial intelligence strategies in high-entropy alloys (2nd Edition), Elsevier, (2019) pp. 81–101
20. M. Xue, X. Mao, Y. Lv, Y. Yong, J. He and Y. Dong, Comparison of micro-nano FeCoNiCrAl and FeCoNiCrMn coatings prepared from mechanical alloyed high-entropy alloy powders, *J. Therm Spray Tech.*, 2021, **30**(6), p 1666–1678.
21. T. M. Butler, Phase stability and oxidation behavior of Al-Ni-Co-Cr-Fe based high-entropy alloys, Ph.D. Thesis, The University of Alabama, (2016).
22. K.-C. Lo, Y.-J. Chang, H. Murakami, J.-W. Yeh and A.-C. Yeh, An oxidation resistant refractory high entropy alloy protected by CrTaO₄-based oxide. *Sci. Rep. Vol.* (2019), pp 7266
23. M. Ma, A. Han, Z. Zhang, Y. Lian, C. Zhao and J. Zhang, The role of Si on microstructure and high-temperature oxidation of CoCr₂FeNb_{0.5}Ni high-entropy alloy coating, *Corr. Sci.*, 2021, **185**, p 109417.
24. J.A. Haynes, M.K. Ferber and W.D. Porter, Thermal cycling behavior of plasma-sprayed thermal barrier coatings with various MCrAlX bond coats, *J. Therm. Spray Technol.*, 2000, **9**(1), p 38–48.
25. C. Zhang, J. Zhu, H. Zheng, H. Li, S. Liu and G.J. Cheng, A review on microstructures and properties of high entropy alloys manufactured by selective laser melting, *Int. J. Extrem. Manuf.*, 2020, **2**, p 1–22.
26. Q. Wu, R. Zhou, Q. Wei, S. Ni, Y. Liu and M. Song, Nanosized precipitates and dislocation networks reinforced c-containing CoCrFeNi high-entropy alloy fabricated by selective laser melting, *Mater. Charact.*, 2018, **144**, p 605–610.
27. D. Lin, N. Zhang, B. He, B. Jin, Y. Zhang, D. Li and F. Dong, Influence of laser re-melting and vacuum heat treatment on plasma-sprayed FeCoCrNiAl alloy coatings, *J. Iron Steel Res. Int.*, 2017, **24**, p 1199–1205.
28. B. Jin, N. Zhang, S. Guan, Y. Zhang and D. Li, Microstructure and properties of laser re-melting FeCoCrNiAl_{0.5}Si_x high entropy alloy coatings, *Surf. Coat. Technol.*, 2018, **349**, p 867–873.

Publisher's Note Springer Nature remains neutral with regard to jurisdictional claims in published maps and institutional affiliations.